ORIGINAL RESEARCH ARTICLE

Oxidative stress-induced RAC autophagy can improve the HUVEC functions by releasing exosomes

Linxin Zhu[1] | Jiankun Zang[2] | Bing Liu[1] | Guocheng Yu[1] | Lili Hao[1] | Lian Liu[1] | Jingxiang Zhong[1]

[1]Department of Ophthalmology, The First Affiliated Hospital of Jinan University, Guangzhou, China

[2]Department of Neurology and Stroke Center, The First Affiliated Hospital of Jinan University, Guangzhou, China

Correspondence
Jingxiang Zhong, MD, PhD, The First Affiliated Hospital, Jinan University, 613 West Huangpu Ave, 510632 Guangzhou, China.
Email: zjx85221206@163.com

Funding information
National Natural Science Foundation of China, Grant/Award Number: 81970806

Abstract

Retinal neovascularization (RNV) is a common pathological feature in many kinds of fundus oculi diseases. Sometimes RNV can even lead to severe vision loss. Oxidative injury is one of the main predisposing factors for RNV occurrence and development. The specific mechanism may be closely related to the special structural tissues of the retina. Retinal astrocytes (RACs) are mesenchymal cells located in the retinal neuroepithelial layer. RACs have an intimate anatomical relationship with microvascular endothelial cells. They have a variety of functions, but little is known about the mechanisms by which RACs regulate the function of endothelial cells. The molecules secreted by RACs, such as exosomes, have recently received a lot of attention and may provide potential clues to address the RAC-mediated modulation of endothelial cells. In this study, we aimed to preliminarily explore the mechanisms of how RAC exosomes generated under oxidative stress are involved in the regulation of endothelial function. Our results showed that the apoptosis and autophagy levels in RACs were positively correlated with the oxidative stress level, and the exosomes generated from RACs under normal and oxidative stress conditions had different effects on the proliferation and migration of endothelial cells. However, the effect of RACs on endothelial cell function could be markedly reversed by the autophagy inhibitor 3-methyladenine or the exosome inhibitor GW4869. Therefore, oxidative stress can lead to increased autophagy in RACs and can further promote RACs to regulate endothelial cell function by releasing exosomes.

KEYWORDS
autophagy, exosome, oxidative stress, retinal astrocytes, tert-butyl hydroperoxide (tBHP)

1 | INTRODUCTION

Ocular neovascularization is a pathological feature of many retinal diseases, especially in retinopathy of prematurity, diabetic retinopathy, and neovascular age-related macular degeneration, and can even lead to vision loss and blindness (van Wijngaarden, Coster, & Williams, 2005). Retinal diseases can be divided into retinal vascular diseases, in which there is leakage and/or neovascularization (NV) from retinal vessels, and subretinal NV, in which new vessels grow into the normally avascular outer retina and subretinal space (Sapieha et al., 2010). The progression of these diseases is related to a variety of cells, but the specific mechanisms involved are still unclear.

Retinal astrocytes (RACs) are the most widely distributed neurogliocytes in the retinal neuroepithelial layer (Jammalamadaka et al., 2015). RACs have many functions, such as participating in the formation of the blood-retinal barrier (Wisniewska-Kruk et al., 2012), transmitting signals, protecting nerve cells (Vecino, Rodriguez, Ruzafa, Pereiro, & Sharma, 2016), and maintaining homeostasis and nutritional support (Provis, 2001). In addition, recent studies have shown that RACs also have a strong secretion function and secrete molecules such as glial cell line-derived neurotrophic factor (Igarashi et al., 2000), nerve growth factor (Castillo et al., 1994), and insulin-like growth factor binding protein-5 (Xu et al., 2010). Targeted protection of RACs can promote normal angiogenesis and inhibit oxygen-induced pathological choroidal NV (Dorrell et al., 2010). Further study suggested that different cell types in the eye may maintain the balance of the ocular vascular environment by secreting angiogenic or inhibitory factors. The results showed that exosomes from normal astrocytes could significantly inhibit choroidal NV, while exosomes extracted from retinal pigment epithelium (RPE) could not (Hajrasouliha et al., 2013); however, the specific mechanism was not clarified in that study.

Exosomes are thought to be used to remove unneeded proteins from the cells. However, recent studies have demonstrated that exosomes are involved in intercellular signal transmission (Meng, Hao, He, Li, & Zhu, 2019). Exosomes from various cell types have been implicated in important physiological and pathological processes, such as antigen presentation, genetic exchange (Murillo et al., 2019), immune responses (Lindenbergh & Stoorvogel, 2018), angiogenesis (Tang, Yue, & Ip, 2018), inflammation (Prattichizzo et al., 2017), tumor metastasis (Matei, Kim, & Lyden, 2017), and pathogen spread. These functions are mainly dependent on the cell condition and the cargo contained within the exosomes (Thery, Ostrowski, & Segura, 2009). A previous study has shown that exosomes from normal astrocytes could significantly inhibit choroidal NV. However, in the course of ocular NV, endothelial cells are not the only pathogenically affected cells, and the role of stressed RACs in disease progression is still a question worth exploring. In the present study, we aimed to determine the function of RAC exosomes on the proliferation, migration, and tube formation of HUVECs under normal and oxidative stress conditions and further explore the mechanism involved in this process. This study may provide a new experimental basis for the occurrence and development of retinal NV and the progression and outcome of choroidal neovascularization and other related research.

2 | MATERIALS AND METHODS

2.1 | Cell culture and treatment

Human retinal astrocytes (hRACs) and human umbilical vein endothelial cells (HUVECs) were purchased from ScienCell (Walkersville, MD). RACs were cultured in AM (astrocyte medium; ScienCell; Cat. No. 1801) supplemented with 2% fetal bovine serum (FBS; ScienCell; Cat. No. 0010), 1% astrocyte growth supplement (ScienCell; Cat. No. 1852), and 1% penicillin–streptomycin (ScienCell; Cat. No. 0503). HUVECs were cultured in MCDB 131 medium (Gibco; Cat. No. 10372019) supplemented with 10% FSB (Gibco, Thermo Fisher Scientific Inc., Waltham, MA; Cat. No. 10099141C), 1% endothelial cell growth supplement (ECGS; ScienCell; Cat. No. 1052), and 1% penicillin-streptomycin (Gibco; Cat. No. 15140122). Both the cell lines were cultured in a humidified 5% CO_2 atmosphere at 37°C.

The oxidative stress cell model was induced by tert-butyl hydroperoxide (tBHP) treatment. In brief, RACs were seeded in culture plates, culture dishes, or upper chamber of the Transwell system. Once they reached 80% confluence, the RACs were washed with phosphate buffered saline (PBS) three times and treated with tBHP, drugs, or dimethyl sulfoxide (DMSO) for several hours. Then, the fresh medium without FBS was replaced, and the cells were washed once. The RACs seeded in the upper chamber of Transwell plates were cocultured with HUVECs after performing the above experiment in new six-well plates.

2.2 | Cell viability tests

2.2.1 | Cell counting kit-8 (CCK-8) assay

RAC survival rates were estimated by the CCK-8 assay (C0038; Beyotime Biotechnology, Shanghai, China). Approximately, 5×10^3 RACs were seeded in 96-well plates with 100 μl medium in each well. After 24 hr of culture, the medium was replaced, and nine different concentrations of tBHP, which were diluted in AM, were added for four different time periods. Then, each well was incubated with 10 μl CCK-8 solution for 2 hr away from light before measuring the absorbance at 450 nm by a Thermo Varioskan LUX Multimode Microplate Reader.

2.2.2 | Lactate dehydrogenase (LDH) assay

We used the LDH assay to measure cell death and cytotoxicity (C0038; Beyotime Biotechnology). Approximately, 0.5×10^4 RACs were seeded in 96-well plates with 100 μl medium in each well. After treating the cells with tBHP, we collected the supernatant for centrifugation to remove the cells. A total of 120 μl/well of supernatant and 60 μl/well LDH working solution were added to 96-well plates and incubated for 30 min at room temperature (approximately 25°C) in the dark before measuring the absorbance at 490 and 600 nm by Thermo Varioskan LUX Multimode Microplate Reader.

2.2.3 | Trypan blue staining

Trypan blue (C0011; Beyotime, Biotechnology) marks dead cells and detects the integrity of the cell membrane. Approximately, 5×10^4 cells were seeded in 24-well plates with 1.5 ml medium in each well. After 24 hr of cultivation, the cells were treated with 15 μM and 30 μM tBHP for 6 hr and then washed with PBS three times. Next, 500 μl trypan blue staining solution was added to each well and washed three times with PBS. The number of blue cells in each well was determined under a microscope.

2.3 | Detection of cellular ROS levels and cell apoptosis level

Reactive oxygen species (ROS) levels after tBHP treatment were quantified using the ROS probe dichloro-dihydro-fluorescein diacetate (DCFH-DA; S0033; Beyotime Biotechnology). RACs were seeded in 10 cm dishes or six-well plates for 24 hr. The cells were treated with tBHP for 6 hr (the cells in 10 cm dishes were collected in EP tubes for flow cytometry detection) and then incubated with 10 μmol DCFH-DA for 30 min at 37°C. The cells were washed three times to remove the extra DCFH-DA. DCFH-DA fluorescence was observed under a fluorescence microscope (Olympus IX71; Tokyo, Japan). Another group of cells seeded onto 10 cm dishes was detected by flow cytometry (Synergy H1; Biotek, Winooski, VT). The excitation wavelength of 2′,7′-dichlorofluorescin diacetate is 488 nm, and the emission is 525 nm.

2.4 | Lipid peroxidation and intracellular glutathione (GSH) detection

Malondialdehyde (MDA) concentration in RACs was detected to evaluate the level of membrane lipid peroxidation (S0131; Beyotime Biotechnology). RACs were lysed in IP Lysis Buffer (87788; Thermo Fisher Scientific). Cell lysates were incubated on ice for 30 min and centrifuged at 15,000g for 15 min at 4°C. Then, 100 μl supernatant was mixed with 200 μl MDA working solution and heated at 100°C for 15 min. After cooling to room temperature, the samples were centrifuged at 1,000g for 10 min. The samples were added to a 96-well plate (200 μl/well), and the absorbance was measured at 532 nm by a Thermo Varioskan LUX Multimode Microplate Reader. The MDA concentration results were calculated from the standard curve and normalized to the sample protein concentration.

Intracellular total GSH was measured using the Total Glutathione Assay Kit (S0052; Beyotime Biotechnology). In brief, the cells were collected by centrifugation at 500g for 5 min and washed three times with PBS. The cells were resuspended three times in the volume of protein-removing buffer S and lysed by repeated cycles of freezing (liquid nitrogen) and thawing (37°C in a water bath). The lysates were centrifuged at 12,000g for 10 min at 4°C, and the supernatants were used for the intracellular total GSH assay. GSH content was expressed as a ratio to the absorbance value at 412 nm of the control cells.

2.5 | Cell migration assay

HUVECs were seeded onto six-well plates at a density of 2.5×10^5 cells/well. After 48 hr of culture, confluence was greater than 80% before the scratch assay. A 200-μl pipette tip was used to press firmly against the top of the tissue culture plate and make a vertical wound by pressing the tip down through the cell monolayer to create three straight lines with two crosses that lacked cells in each well, and the debris was removed by PBS. New MCBD medium with ECGS, RAC-derived exosomes or PBS was added to the cells. The exosomes were added to the medium at approximately 5,000 times to the number of cells. Eight images of each well were captured immediately after scraping and after a 12- and 24-hr incubation period. The areas without cells were measured using ImageJ.

For the cell migration assay in the coculture system, we first used six-well Transwell plates with 24 mm inserts with 0.4 μm polyester membrane permeable supports (Corning). In the upper chamber, we seeded RACs at a density of 6×10^{4}, and in the lower chamber, we seeded HUVECs at a density of 2.5×10^5 cells/well. Once the RACs reached confluence, we treated RACs with 30 μM tBHP or DMSO for 6 hr, then 3-methyladenine (3MA) was added or not after wounding. At that time, the HUVECs were greater than 80% confluent before the scratch assay. We put the upper chamber into the coculture system. The remaining steps were performed as previously described.

2.6 | Tube formation assay

A total of 1.3×10^5 HUVECs/well were seeded into 24-well plates precoated with Matrigel (BD Biosciences). The plates were incubated for 12 hr with different treatments to evaluate the formation of tube-like structures. As a negative control, HUVECs were incubated in MCDB without supplements or FBS; as a positive control, the cells were incubated in MCDB with 0.5% (0.25%) ECGS. For experimental treatments, HUVECs were incubated in MCDB treated with RAC-derived exosomes from different conditions. The exosomes were added to the medium at approximately 5,000 times to the number of cells. After 12 hr of incubation, the numbers of tubes of the five groups were counted from three different viewing fields at ×10 magnification using a microscope (Leica DM6000). Eight images of each well were captured and measured using ImageJ.

For the cell migration assay in the coculture system, we used 24-well Transwell plates with 6.5 mm inserts with 0.4 μm polyester membrane permeable supports (Corning). In the upper chamber, we seeded RACs, and in the lower chamber, we seeded HUVECs. First, we seeded RACs in the inserts, and once they reached confluence, we treated the two groups with 30 μm tBHP for 6 hr. After that, a total of 1.3×10^5 HUVECs/well were seeded in the bottom chambers of the 24-well plates precoated with Matrigel in FBS-free-MCDB medium with or without ECGS, and the inserts with RACs were

TABLE 1 Information of the primary antibodies used in this study

Antibody	Specificity	Type	Item numbers	Dilution	Source
β-Actin	β-Actin	Monoclonal	#3700	1:10,000 WB	Cell Signaling
Bcl-2	Total Bcl-2	Polyclonal	#15071 S	1:1,000 WB	Cell Signaling
Caspase 3	Total caspase 3	Polyclonal	#9662	1:1,000 WB	Cell Signaling
Cleaved caspase 3	Cleaved caspase 3	Polyclonal	#9664	1:1,000 WB	Cell Signaling
mTOR	Total mTOR	Polyclonal	#2983	1:1,000 WB	Cell Signaling
p-mTOR	p-mTOR at Ser2448	Polyclonal	# 5536	1:1,000 WB	Cell Signaling
P62	SQSTM1/p62	Polyclonal	#23214	1:1,000 WB	Cell Signaling
LC3α/β	LC3A/B	Polyclonal	#4108	1:1,000 WB	Cell Signaling
LC3β	LC3B	Polyclonal	#2775	1:100 IF	Cell Signaling
GFAP	GFAP	Polyclonal	#80788	1:50 IF	Cell Signaling
LAMP1	LAMP1	Monoclonal	#9091	1:100 IF	Cell Signaling
Cyclin D1	Cyclin D1	Monoclonal	#55506	1:1,000 WB	Cell Signaling
FAK	Total FAK	Polyclonal	#71433	1:1,000 WB	Cell Signaling
p-FAK	p-FAK at Try397	Polyclonal	#8556	1:1,000 WB	Cell Signaling
Src	Total Src	Polyclonal	# 2108	1:1,000 WB	Cell Signaling
p-Src	p-Src at Try416	Polyclonal	PA5–97364	1:50 IF	Thermo Fisher
Akt	Total Akt	Monoclonal	#4691	1:1,000 WB	Cell Signaling
p-Akt (Ser473)	p-Akt at Ser473	Polyclonal	#4060	1:1,000 WB	Cell Signaling
CD34	CD34	Polyclonal	ab81289	1:100 IF	Abcam
CD63	CD63	Polyclonal	ab59479	1:1,000 WB /1:100 IF	Abcam
VE-Caherin	VE-Caherin	Polyclonal	ab33168	1:100 IF	Abcam
HSP70	HSP70	Monoclonal	#4873	1:1,000 WB	Cell Signaling
TSG101	TSG101	Polyclonal	ab125011	1:1,000 WB /1:100 IHC	Santa Cruz

Abbreviations: Bcl-2, B-cell lymphoma 2; FAK, focal adhesion kinase; GFAP, glial fibrillary acidic protein; IF, immunofluorescence; IHC, immunohistochemistry; LAMP1, lysosome-associated membrane protein 1; LC3A/B, light chain 3α/β; mTOR, mammalian target of rapamycin; p, phosphorylated; WB, western blot analysis.

placed on top of the HUVEC wells at the same time. The remaining steps were performed as described.

2.7 | Cell immunofluorescence

The cells seeded in confocal dishes were fixed with 4% paraformaldehyde and then incubated in 0.5% Triton for 15 min to rupture the cell membranes. Following three PBS washes, nonspecific antigen-binding sites were blocked with 5% BSA for an hour. The RACs were then incubated with primary antibodies (Table 1) overnight at 4°C. After washing, the cells were incubated with anti-rabbit or anti-mouse fluorescently labeled antibody for 60 min at room temperature, and the nuclei were stained with 4',6-diamidino-2-phenylindole for 2 min, which was washed with PBS afterwards. The cells were kept from light before observation with a fluorescence microscope.

2.8 | Western blot analysis

Cells and exosomes were lysed in RIPA (P0013D; Beyotime Biotechnology) buffer supplemented with 1x Protease Inhibitor Cocktail (20-116; Millipore) and centrifuged at 12,000 rpm for 15 min at 4°C. The supernatant was collected, and the total protein content was determined by a BCA Protein Assay Kit (23225; Thermo Fisher Scientific). Proteins were separated on 10% sodium dodecyl sulfate-polyacrylamide gels and transferred to a 0.22 μm nitrocellulose (NC) membrane. Membranes were blocked with 5% fat-free milk (5% skimmed milk, 0.1% Tween in TBST) and incubated with primary antibodies (Table 1) overnight at 4°C. After being washed five times with TBST for 10 min, the membranes were incubated with secondary antibodies for 1 hr at room temperature. Following washing, the target bands were visualized using Tanon-5200 Image Analyzer. All bands were quantified by ImageJ and normalized to β-actin and the fold changes were calculated through relative quantification to the control group.

2.9 | Transmission electron microscopy

Cells were fixed by immersion in 2.5% glutaraldehyde in 0.1 M Sorensen buffer, post-fixed in 1% osmium tetroxide, and stained in 3% uranyl acetate. Then, the cells were dehydrated in ethanol and embedded in Epon. Ultra-thin sections were post-stained with uranyl acetate and lead citrate and examined using a Philips CM100 electron microscope at 60 kV. Images were recorded digitally with a Kodak 1.6 Megaplus camera system operated using AMT software (Advanced Microscopy Techniques, Danvers, MA).

2.10 | Isolation and characterization of exosomes

The cells described above were grown to confluence in AM. After modeling, the FBS-free AM was added to RACs for 24 hr, and then exosomes were purified from the culture supernatant using the same sequential centrifugation procedure described previously (H. F. Wang et al., 2018). In brief, the medium was centrifuged at 300g for 10 min to remove the cells. The supernatant was centrifuged at 2000g for 10 min and then at 10,000g for 30 min. The resulting supernatant was filtered through a 0.22-μm filter and centrifuged at 100,000g for 2 hr at 4°C (Beckman Type 90 Ti). Then, the exosome pellet was resuspended in 100 μl PBS and stored at −80°C.

For electron microscopy, a 10-μl aliquot of freshly isolated exosomes was loaded onto Formvar carbon-coated grids and negatively stained with 2% uranyl acetate. The grids were examined with an FEI Tecnai G2 Spirit transmission electron microscope (TEM; FEI Europe, Eindhoven, The Netherlands), and the images were recorded using a Morada CCD camera (Olympus Soft Image Solutions GmbH, Münster, Germany).

For NanoSight tracking analysis, the number and size of the exosomes were directly tracked using an NS300 instrument (Malvern Instruments Ltd., Worcestershire, UK). In this analysis, particles are automatically tracked and sized based on the Brownian motion and the diffusion coefficient. The exosomes were diluted 50 times in PBS to obtain a concentration suitable for detection. The samples were loaded into the sample chamber at an ambient temperature. Three 30-s videos were acquired for each sample. The videos were subsequently analyzed with the NTA 2.3 software, which identified and tracked the center of each particle under Brownian motion to measure the average distance the particles moved on a frame-by-frame basis.

2.11 | Statistical analysis

Data are expressed as mean ± standard deviation (SD) and analyzed using SPSS 12.0 statistical software (SPSS Inc., IL). A one-way analysis of variance, followed by least significant difference post hoc tests, was used to determine the statistical significance of the means. The post hoc tests used were the LSD and Bonferroni statistical tests, and the choice of post hoc test depended on the p value of the homogeneity of variances. The LSD statistical tests were used when this p value was >.05. Otherwise, we used the Bonferroni statistical test. The level of significance for all analyses was set at $p < .05$.

3 | RESULTS

3.1 | tBHP induces oxidative stress injury and increases apoptosis and autophagy levels in RACs

Treatment with tBHP was used in the present study to induce oxidative stress in RACs, and the efficiency of this model was evaluated in Figure 1. Based on the CCK-8 and LDH release assay results, the cell viability declined with increasing drug concentrations for different exposure times. Slow damage at low concentrations can cause adaptive changes in the cell and stabilize the model. In the present study, we found that after 6 hr of treatment, 15 and 30 μM tBHP led to 75% and 55% cell viability, respectively (Figure 1a). In addition, 30 μM treatment induced a 1.5-fold increase in LDH release (Figure 1b). The trypan blue staining and bright field images also suggested that treatment with tBHP could induce obvious continuous changes in cell morphology and membrane permeability at the two concentrations when compared with the control group (Figure 1c). This is consistent with the results of apoptosis measured by flow cytometry, whereby the rate of apoptosis was increased significantly after treatment with tBHP (Figure 1d). To further verify that this damage was caused by oxidative stress, we first tested the GSH concentration and cellular MDA level, which can assess the levels of antioxidant production and membrane lipid peroxidation, respectively (Figure 1e and 1f). The results showed that as the intracellular total GSH declined with the tBHP concentration, the MDA level increased significantly. The ROS level reflected by DCHA-DA staining in the cells was tested by flow cytometry analysis and immunofluorescence. The results suggested that 15 μM tBHP significantly increased the intracellular ROS concentration, and 30 μM tBHP induced an almost 2-fold elevation in ROS levels compared with those in normal cells (Figure 1g–i). Thus, tBHP can cause significant oxidative stress damage in RACs, and we chose 15 and 30 μM treatments for mild and severe damage, respectively.

In addition, apoptosis and autophagy levels were detected in tBHP-treated RACs. As shown in Figure 2a,b, as the expression of cleaved caspase 3 and Bax increased in cells treated with tBHP, B-cell lymphoma 2 (Bcl-2) expression was obviously decreased, and the number of TUNEL-positive cells was highly increased in both the low-dose and high-dose tBHP treatment groups, which indicated that the apoptosis level of the cells was positively correlated with tBHP treatment in a dose-dependent manner.

In Figure 2c,d, the western blot and immunofluorescence results indicated that LC3β expression was highly elevated, which accompanied with the p62 declined, in the tBHP groups. The phosphorylation of mammalian target of rapamycin (mTOR) was downregulated in the tBHP-treated cells. Besides, based on the scanning electron microscope images (Figure 2f), we found that there was a significant
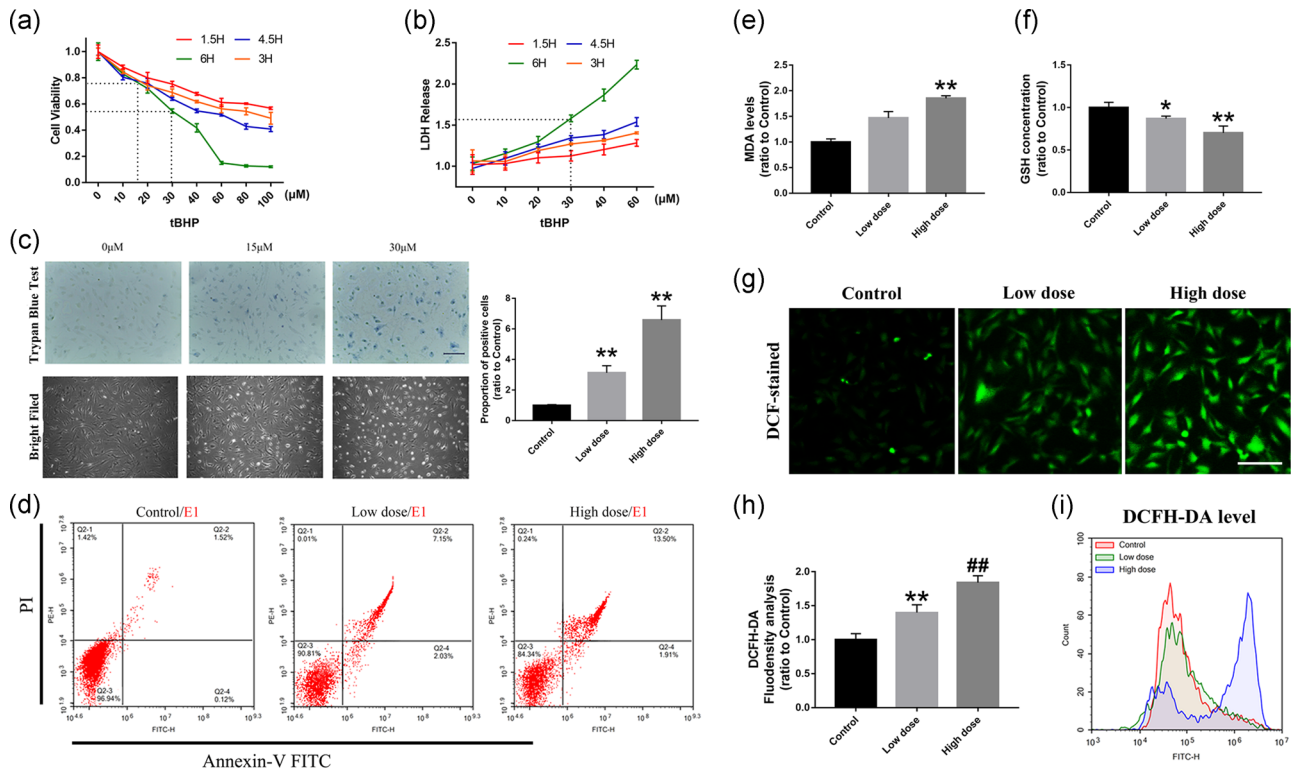
FIGURE 1 tBHP can induce oxidative stress damage in RACs. (a,b) The CCK-8 and LDH results of RACs treated with different tBHP concentrations. The 15 and 30 μM tBHP led to 75% and 55% cell viability, respectively. (c) Trypan blue staining and bright field imaging of RACs under 15 μM (low dose) and 30 μM (high dose) tBHP treatment. The number of positively stained cells was highly increased and the low tBHP-treated cells showed a significant change in cell morphology. (d) Flow cytometry detection of cell apoptosis in the low-dose and high-dose tBHP treatment groups by annexin V–FITC staining. Significant increase in apoptosis level can be observed in the low dose-treated groups. (e,f) The results of intracellular MDA levels and GSH concentrations in low-dose tBHP-treated RACs. MDA increased with increasing tBHP concentrations, and GSH declined as the drug dose increased. (g–i) DCFH-DA immunofluorescence staining and flow cytometry detection of RACs under different tBHP treatments. Intracellular ROS levels and DCFH-DA-positive cells were significantly enhanced by tBHP. Scale bar = 100 μm. The results are expressed as mean ± standard deviation. CCK-8, cell counting kit-8; DCFH-DA, dichloro-dihydro-fluorescein diacetate; FITC, fluorescein isothiocyanate; GSH, glutathione; LDH, lactate dehydrogenase; MDA, malondialdehyde; RAC, retinal astrocyte; ROS, reactive oxygen species. $*p < .05$ and $**p < .01$ versus control; and $^{\#\#}p < .01$ versus Low dose

change in the mitochondrial morphology in tBHP-treated RAC. The cristae (inner membrane) of the mitochondria were destroyed and the boundaries were unclear. The severely damaged mitochondria were vacuolated, only retaining part of the intima and contours. Moreover, both the early autophagosomes (marked by symbol "#") and autolysosome (late autophagosomes, marked by symbol "*") can be observed in the two tBHP-treated groups. According to the previous study, it is known that the late autophagosome which fuses with the lysosome to form the autolysosome and resolve the content (Jeppesen et al., 2019). Moreover, LAMP1 is a specific marker of the lysosome, and the colocalization of LC3β and LAMP1 can also reflect the cell autophagy level (B. Guo et al., 2014). In our study, the number of autolysosomes stained by LAMP1 and LC3β was significantly increased in tBHP-treated RACs and was positively correlated with the drug concentration (Figure 2e). These results are highly consistent with autophagic flow enhancement. Therefore, tBHP treatment led to an increase in intracellular ROS levels, which caused a significant increase in intracellular apoptosis and autophagy levels. As the 30 μM group had a more obvious autophagy and apoptosis increase than the

15 μM group, we selected the 30 μM tBHP treatment for subsequent experiments.

3.2 | RAC autophagy levels can influence HUVEC proliferation and migration in a coculture system

To investigate the effect of RACs under different conditions on endothelial cells, we established a Transwell system to study the effects of RACs on HUVEC function (Figure 3a). Compared with the ECGS group, the branching points and lumen count in the ECGS + control RACs were significantly decreased, and the cell mobility was obviously decreased, which suggested that under normal conditions RACs strongly inhibited HUVEC tube formation and migration. However, after treatment with tBHP, when compared with the no ECGS group, tBHP-RACs obviously increased tube formation and endothelial cell migration in the Transwell assay (Figure 3c). Based on the previous results, tBHP can induce a significant increase in RAC autophagy. 3MA has been used to block the autophagy response in
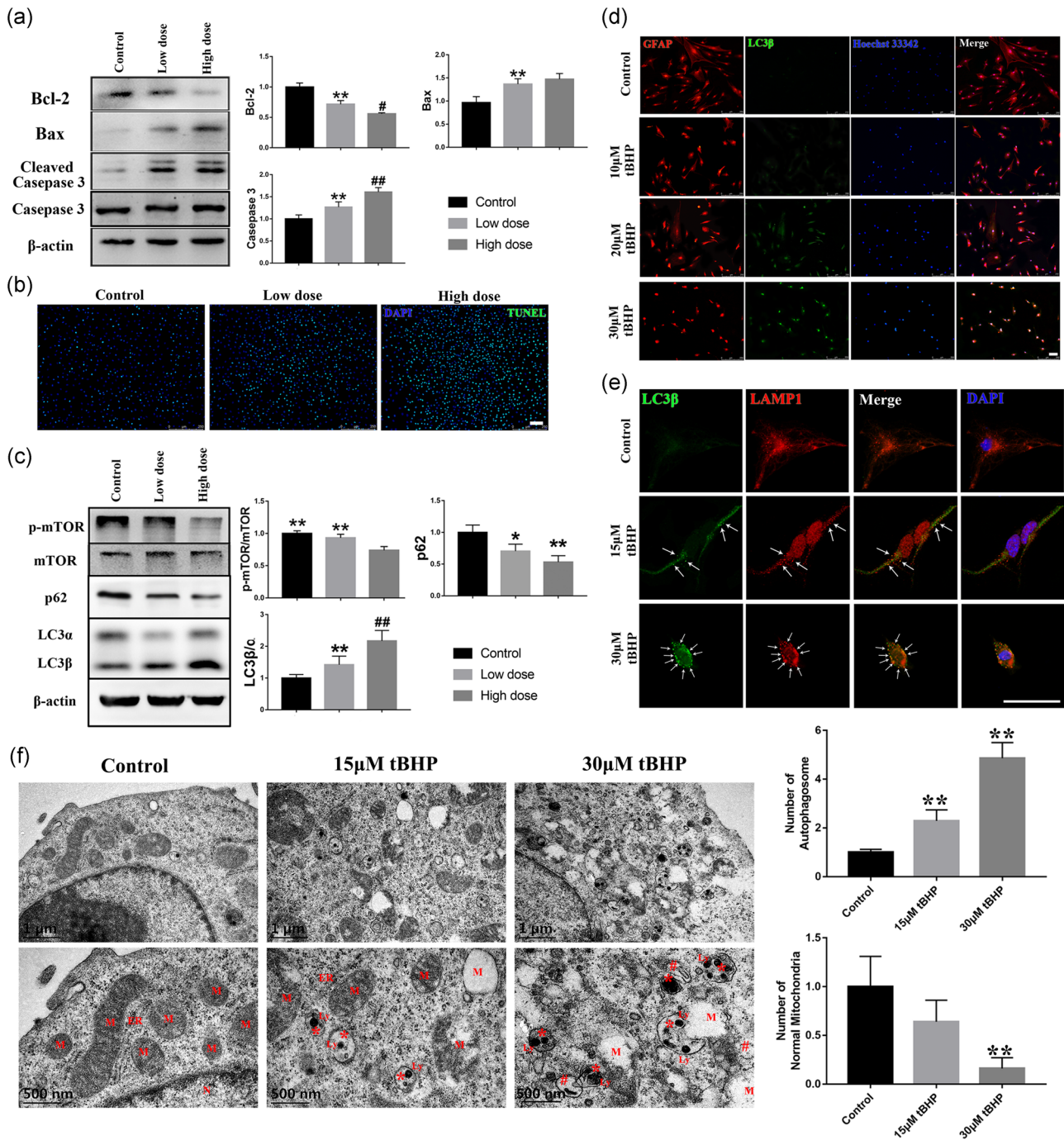
FIGURE 2 The oxidative stress induced by tBHP can have a dose-dependent effect on apoptosis and autophagy in RACs. (a,b) The activity of the mitochondrial apoptosis pathway Bcl-2-Bax-caspase 3 was highly enhanced by tBHP. The number of TUNEL-positive cells increased as the oxidative stress increased. (c,d) The autophagy pathway mTOR-p62-LC3 was activated by the oxidative stress induced by tBHP. The number of LC3β-positive cells increased as the oxidative stress increased. (e) The number of autolysosomes was significantly increased in the two tBHP-treated groups, which can be seen as a late morphology of autophagosomes and labeling by LC3β and LAMP1 (white arrow). (f) The scanning electron microscope images of three groups. With the increase of tBHP concentration, the number of normal mitochondria decreased significantly and was accompanied by an increase in the number of autophagosomes. ER, endoplasmic reticulum; N, nuclear; M, mitochondria; Ly, lysosomal; * is for early autophagosomes; # is for autolysosomes. Scale bar = 100 μm. The results are expressed as mean ± standard deviation. Bax, Bcl-2 associated X protein; Bcl-2, B-cell lymphoma 2; ER, endoplasmic reticulum; LAMP1, lysosome-associated membrane protein 1; LC3β, light chain 3β; Ly, lysosomal; M, mitochondria; N, nuclear; RAC, retinal astrocyte; tBHP, tert-butyl hydroperoxide; TUNEL, terminal deoxynucleotidyl transferase biotin-dUTP nick end. *$p < .05$ and **$p < .01$ versus the control; #$p < .05$ and ##$p < .01$ versus the low-dose group
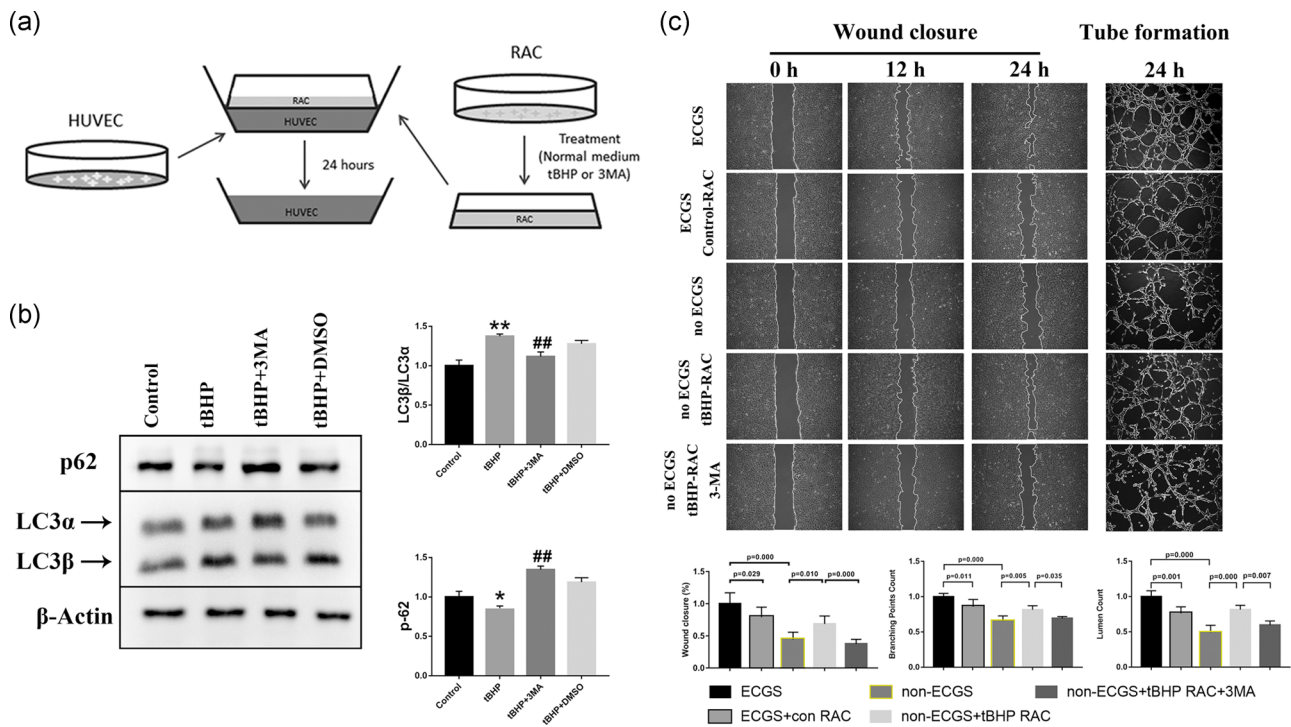
FIGURE 3 RACs have different effects on HUVEC tube formation and migration under different autophagy levels in coculture systems. (a) The diagram for establishing a coculture system for RACs and HUVECs. (b) tBHP could increase the LC3β/LC3α ratio and decrease p62 expression, while this effect was reversed by 3MA treatment. (c) The wound closure and tube formation assays of HUVECs cocultured with normal or tBHP-treated RACs at different time points. The normal RACs could block the ECGS improvement on HUVEC function. However, the oxidative stress RACs treated with tBHP led to a significant elevation in HUVEC tube formation and migration in the no ECGS group. After inhibiting RAC autophagy by 3MA, the enhancement of tBHP RACs on HUVECs was obviously reduced. The results are expressed as mean ± standard deviation. 3MA, 3-methyladenine; ECGS, endothelial cell growth supplement; HUVEC, human umbilical vein endothelial cell; LC3α, light chain 3α; LC3β, light chain 3β; RAC, retinal astrocyte; tBHP, tert-butyl hydroperoxide. *$p < .05$ and **$p < .01$ versus the control; ##$p < .01$ versus the tBHP group

RACs, and we used 3MA to further explore the role of RAC autophagy in the regulation of HUVEC functions. We first assessed the effect of 3MA on RACs. Western blot results showed that 3MA could obviously decrease the tBHP-induced induction of autophagy. Compared with the effect on HUVECs cocultured with tBHP-RACs, decreasing RAC autophagy by 3MA significantly decreased HUVEC function in terms of both tube formation and migration (Figure 3b).

Tube formation and migration of endothelial cells are closely related to the Src–FAK–Akt–mTOR pathway, which is involved in proliferation and migration. As shown in Figure 4a, the phosphorylation levels of FAK, Src, Akt, and mTOR were significantly decreased in the control-RAC group compared with the ECGS group, and we observed a similar decline in cyclin D1 expression. This result indicates that the activity of the Src–FAK–Akt–mTOR pathway was blocked in the control RACs. In addition, the tBHP-treated RACs had a completely opposite effect on HUVECs and induced a significant elevation in Src–FAK–Akt–mTOR pathway activation and cyclin D1 expression. This finding was highly consistent with the tube formation and wound closure results. Nevertheless, 3MA could remarkably block the tBHP-RAC-induced improvement of HUVEC function. The immunofluorescence results presented the same phenomenon

(Figure 4b). Compared with the ECGS group, the HUVECs cocultured with the control RACs had a lower phosphorylation of Src, but the tBHP-treated RACs significantly increased the phosphorylation of Src in the no ECGS HUVECs, and 3MA reversed the effect of tBHP-RACs. Therefore, the results suggested that normal RACs inhibited the proliferation and migration of HUVECs and that the tBHP-induced increase in autophagy could obviously enhance HUVEC proliferation and function by the Src–FAK–Akt–mTOR pathway. Blocking the autophagy response could impair the effect of tBHP-RACs on HUVEC function.

VE-cadherin is known to be required for maintaining a restrictive endothelial barrier. Integrity of intercellular junctions is a major determinant of permeability of the endothelium, and the VE-cadherin-based adherens junction is thought to be particularly important (Corada et al., 2001). In the present study, compared with the ECGS-treated HUVEC, the expression and distribution of VE-cadherin in HUVEC can be obviously declined when cocultured with normal RAC. On the other hand, the tBHP-treated RAC can significantly elevate the VE-cadherin expression and the distribution between the HUVEC when compared with no ECGS group. And the 3MA can block this tBHP-RAC effect on HUVEC.
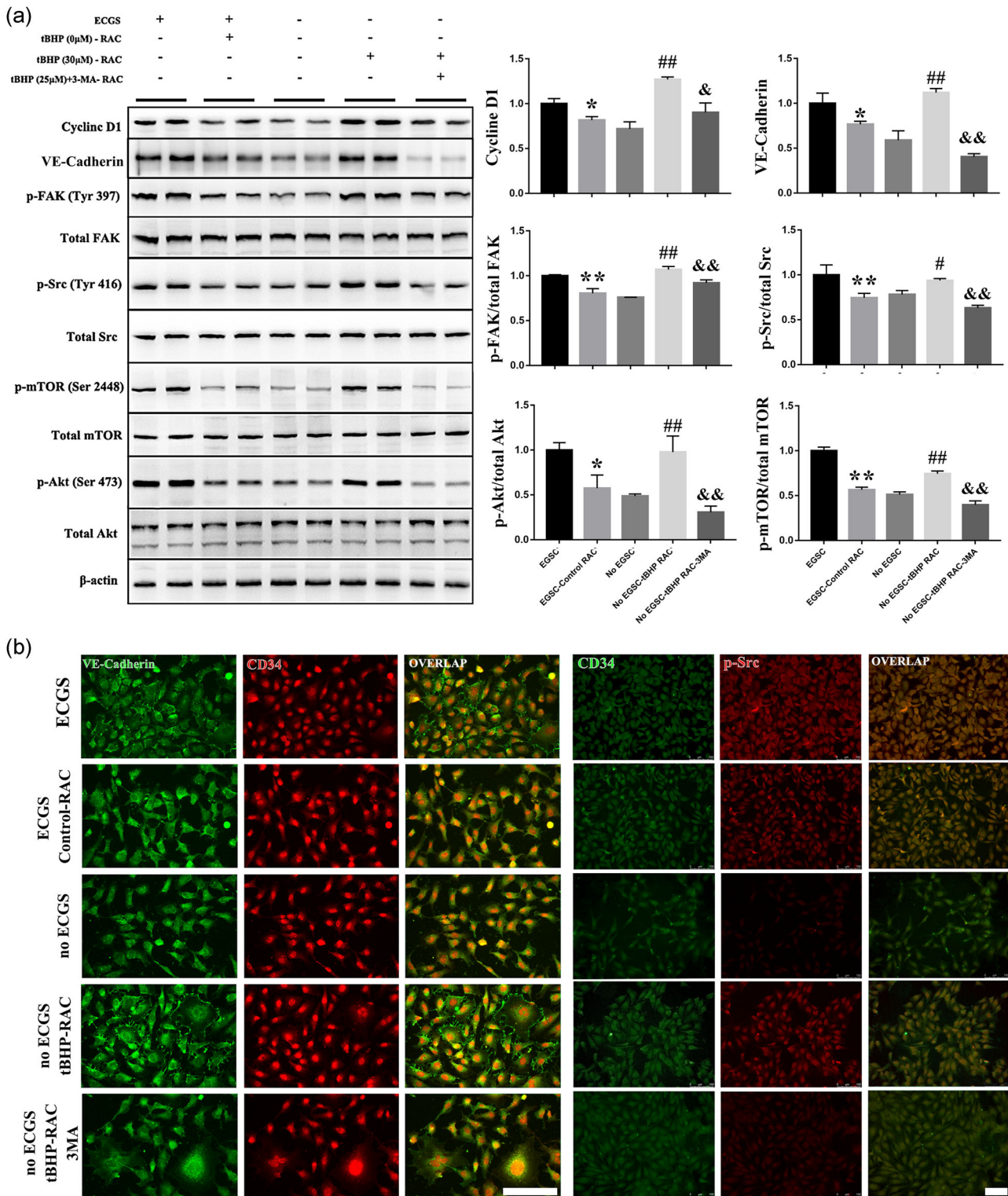
FIGURE 4 The proliferation- and migration-related pathways in HUVEC are highly inhibited by normal RACs and enhanced by high-autophagy levels RACs in a coculture system. (a,b) The activity of the Src–FAK–Akt–mTOR pathway and expression of cyclin D1 and VE-cadherin were decreased by normal RACs when compared with the ECGS groups. However, tBHP-RACs can clearly increase the pathway activity and expression of cyclin D1 and VE-cadherin compared with the no ECGS group. Moreover, 3MA can block the tBHP-RAC effects on the related pathway in HUVECs. Scale bar = 100 μm. The results are expressed as the mean ± standard deviation. 3MA, 3-methyladenine; ECGS, endothelial cell growth supplement; FAK, focal adhesion kinase; HUVEC, human umbilical vein endothelial cell; mTOR, mammalian target of rapamycin; RAC, retinal astrocyte; tBHP, tert-butyl hydroperoxide; VE, vascular endothelial. $*p < .05$ and $**p < .01$ versus ECGS; $\#p < .05$ and $\#\#p < .01$ versus no ECGS; $\&p < .05$ and $\&\&p < .01$ versus the no ECGS-tBHP RAC group

3.3 | The exosomes generated from RACs under different conditions have different effects on HUVEC function

As autophagosomes and exosomes have a close relationship in their generation and processing (Figure 5a), we further tested the coexpression of the marker of exosomes or their precursors CD63 with the autophagosome marker LC3β (Figure 5b). The immunostaining results showed that part of the CD63 molecule can be completely coexpressed with LC3β. Furthermore, we compared the relevant characteristics of exosomes generated from control-RAC, tBHP-RAC, and tBHP-3MA-RAC. The particle size of the microvesicles
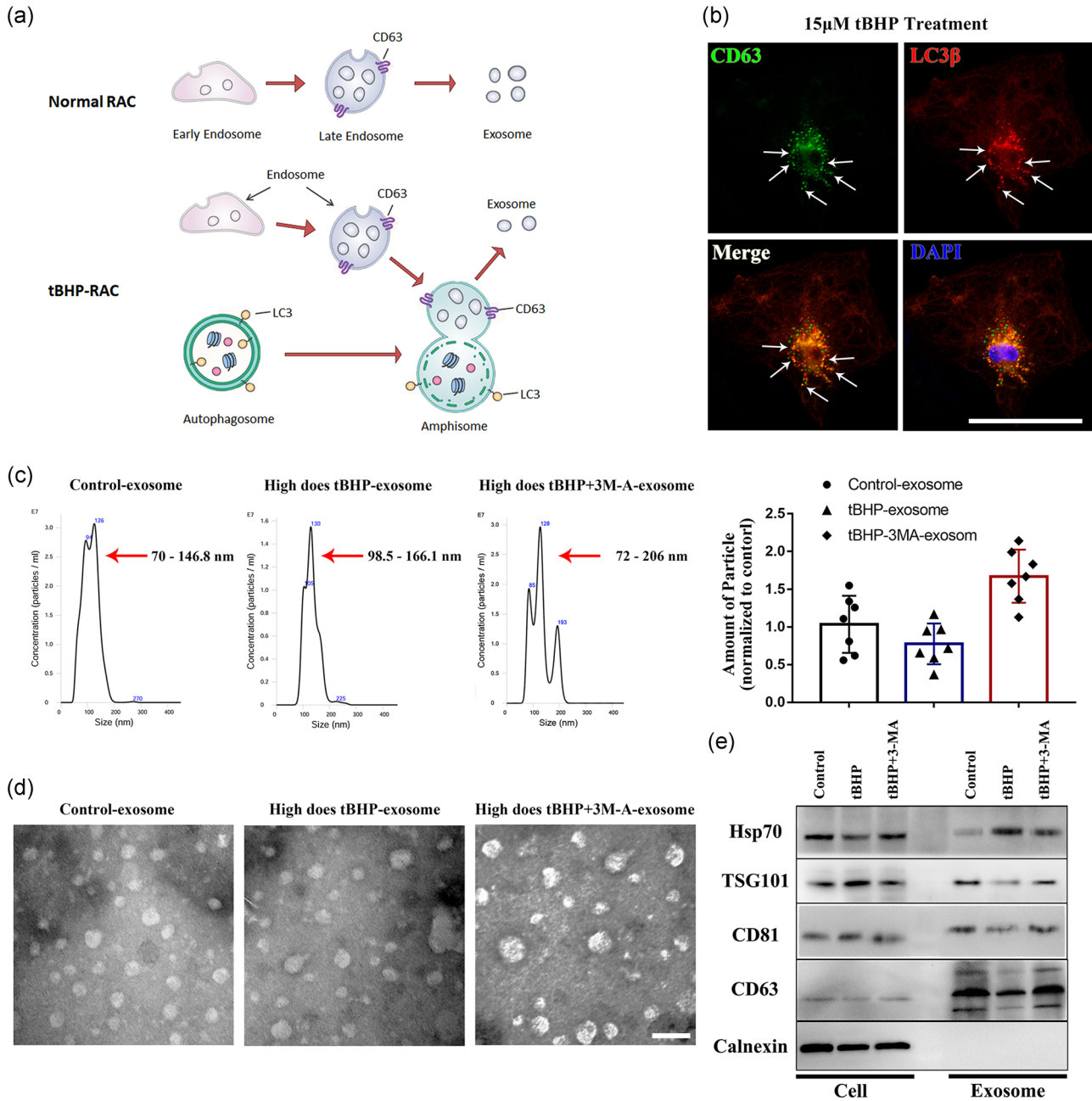

FIGURE 5 The exosomes generated from normal RACs, tBHP-treated RACs, and tBHP+ 3MA-treated RACs show significant differences. (a) The process of exosome formation in normal cells or high-autophagy level cells. (b) Amphisomes labeled by CD63 and LC3β can be observed in tBHP-treated RACs (white arrows). (c,d) NanoSight analysis and transmission electron microscopy images of normal, tBHP- and tBHP+ 3MA-treated RAC-derived exosomes. The normal RAC-derived exosomes had a smaller size and higher concentration than the tBHP-RAC-derived exosomes. The 3MA can further enlarge the particle size and elevate the concentration. (e) Western blot results of the exosome biomarker in cells and exosome samples. The expression of HSP70, TGS101, CD81, and CD63 was obviously different between the control, tBHP, and tBHP + 3MA exosomes. Scale bar = 100 μm in the immunofluorescence images; scale bar = 200 nm in the transmission electron microscopy images. 3MA, 3-methyladenine; CD63, cluster of differentiation 63; CD81, cluster of differentiation 81; HSP70, 70 kDa heat shock protein; LC3β, light chain 3β; RAC, retinal astrocyte; tBHP, tert-butyl hydroperoxide; TGS101, tumor susceptibility gene 101

was detected by NanoSight. The result in Figure 5c showed that most microvesicles in the control-RAC group had a particle size between 70 and 146.8 nm, the microvesicles in tBHP-treated RACs had a particle size from 99.5–166.1 nm and 72–206 nm in tBHP + 3MA treated RACs generated microvesicles. These were consistent with the range of exosome size, and the tBHP-RAC-derived exosomes had a larger size and a smaller quantity than the control-derived exosomes. Blocking the autophagy response by 3MA in RACs can further enlarge the exosome size and increase the number of particles. TEM images also indicated that the morphology and size of the microvesicles were highly matched with the characteristics of exosomes. Meanwhile, it also indicated that the tBHP-RAC-derived exosomes had larger sizes than the control exosomes and 3MA can further increase the particle size (Figure 5d). Moreover, to further verify the properties of the extracted microvesicles, we tested specific exosome markers. The western blot result in Figure 5e suggested that the exosome biomarkers HSP70, TSG101, CD81, and CD63 were enriched in the exosome sample, but the calnexin level in the exosome sample, which is expressed on the endoplasmic reticulum membrane, was far less than that of the cell lysate sample. Compared with the exosomes generated from the tBHP-treated cells, the control-RAC-derived exosomes had higher expression of TSG101, CD81, and CD63 and lower expression of HSP70. Meanwhile, 3MA can reverse the effects of tBHP on those proteins. This part of the result indicated that the exosomes produced from the control and tBHP RACs have different features, and tBHP-induced autophagy may involve in the exosomal contents packaging and exosome synthesis in RAC.

After RAC-exosome isolation, we further examined their effects on HUVECs (Figure 6a). By adding the exosomes to the medium, we found that the normal RAC-exosomes could reduce the lumen count and branching points in the tube formation assay, and the migration of HUVECs was also highly reduced in the wound closure test (Figure 6c). This result indicated that normal RAC-exosomes could reverse the ECGS-induced promotion of HUVEC function, and the phenomenon was consistent with the ECGS-control-RAC-HUVEC co-culture results. Furthermore, compared with the no ECGS group, the exosomes extracted from tBHP-treated RACs showed a remarkable enhancement of tube formation and increased the migration of HU-VECs, which presented an even stronger effect than the ECGS only group and was consistent with the Transwell system results
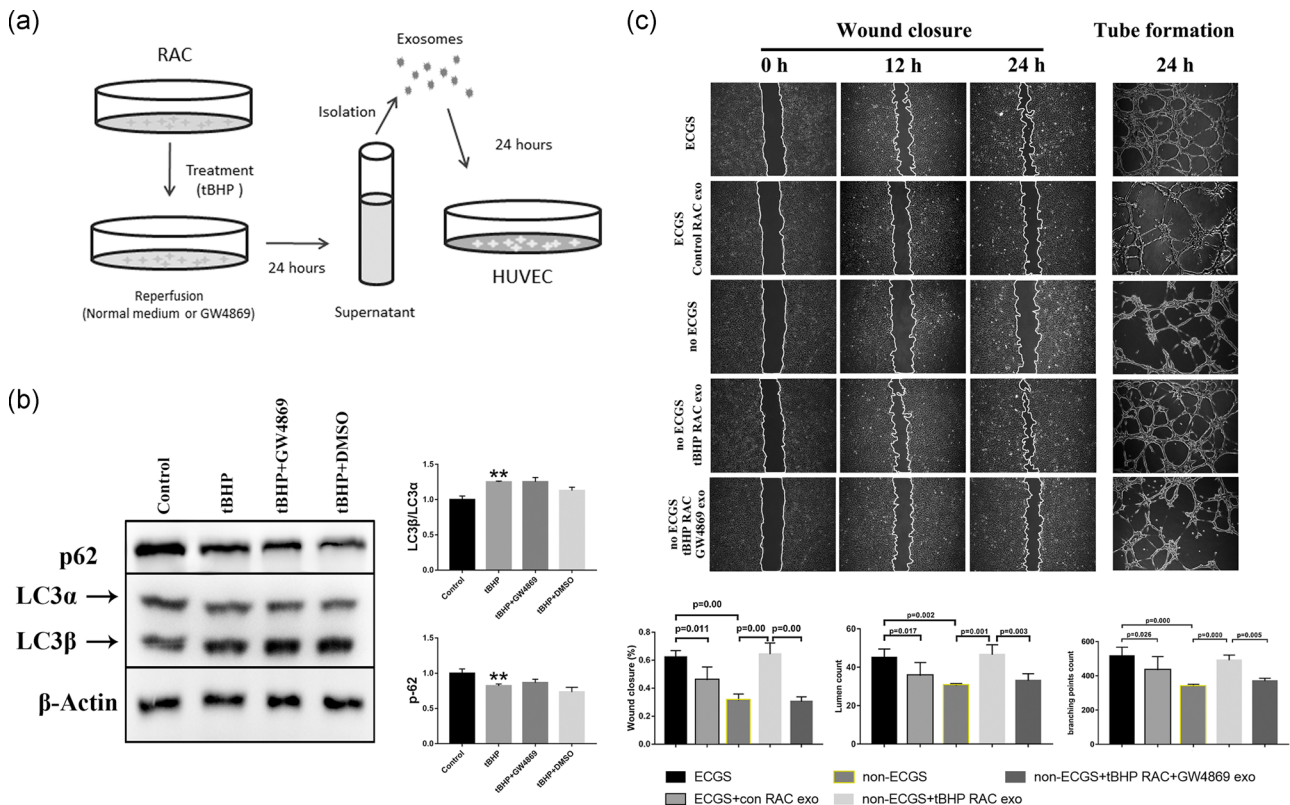

FIGURE 6 The exosomes isolated from normal or tBHP-treated RACs have different effects on HUVEC tube formation and migration, and this effect can be reduced by GW4869. (a) A diagram demonstrating the effect of different RAC-derived exosomes on endothelial function. (b) GW4869 does not affect the LC3β/LC3α ratio or p62 expression in tBHP-RACs. (c) Wound closure and tube formation assays of HUVECs treated with normal or tBHP RAC-derived exosomes at different time points. The normal RAC-generated exosomes can block the ECGS-induced improvement of HUVEC function. However, exosomes obtained from oxidative stress RACs can lead to a significant elevation in HUVEC tube formation and migration in the no ECGS group. After inhibiting the exosome release by GW4869, the enhancement effect of tBHP RAC exosomes on HUVECs was obviously reduced. The results are expressed as mean ± standard deviation. ECGS, endothelial cell growth supplement; HUVEC, human umbilical vein endothelial cell; RAC, retinal astrocyte; tBHP, tert-butyl hydroperoxide. **$p < .01$ versus the control

(Figure 6c). This means that the addition of RAC-exosomes had a similar effect as RAC coculture treatment. To further confirm the exosome function in HUVEC regulation by RACs, we used the exosome inhibitor GW4869. According to the western blot results in Figure 6b, GW4869 had no significant effect on RAC autophagy responses. However, the lumen count and branching points of HUVECs in tube formation assays were significantly reduced after blocking the tBHP-RAC exosome generation by GW4869. The wound closure assay showed that the tBHP-RAC enhancement of HUVEC migration was also downregulated by GW4869 (Figure 6c). Thus, this result suggested that the exosome might function as a key role in RAC regulating HUVEC function.

The pathway associated with tube formation and migration of HUVECs was also investigated. We further tested the activity of this pathway and the expression of the cyclin D1 and VE-cadherin (Figure 7a). As expected, the abundance of cyclin D1, VE-cadherin, and the phosphorylation of Src, FAK, Akt, and mTOR were obviously reduced by normal RAC exosomes compared with the ECGS group. The exosomes produced by tBHP-RACs could significantly improve the phosphorylation level of these molecules and elevate cyclin D1 and VE-cadherin expression. Moreover, inhibition by GW4869 inhibited the activation of this pathway and the increase in cyclin D1 and VE-cadherin in tBHP-RAC exosomes treated group. Similar results were obtained with immunofluorescence (Figure 7b). Compared with the ECGS group, the normal RAC-exosome-treated HUVECs had a lower phosphorylation of Src and less distribution of VE-cadherin, but the tBHP-RAC exosome treatment significantly increased the phosphorylation of Src and VE-cadherin in the no ECGS HUVECs, and GW4869 reversed the effect of tBHP-RAC-derived exosomes. This result further confirmed that by releasing exosomes, RACs are involved in the regulation of HUVEC function through the Src–FAK–Akt–mTOR pathway.

4 | DISCUSSION

4.1 | Oxidative stress and RACs

ROS play an important role in the pathogenesis and development of many ocular diseases. Some studies have shown that ROS are closely related to corneal NV (Henkind, 1964), dry eye (Seen & Tong, 2018), cataract (Periyasamy & Shinohara, 2017), glaucoma (Lin & Kuang, 2014), and retinal degeneration (Zhang et al., 2013). ROS are generated by exogenous and endogenous factors, such as hyperglycemia, drug, and ultraviolet injury (Ung et al., 2017). In some retinal vascular-related diseases, when ROS production exceeds the detoxification and scavenging capacity of the cells, the oxidative stress ensues, which further promotes the expression of intercellular adhesion molecules in endothelial cells (Santiago, Boia, Aires, Ambrosio, & Fernandes, 2018). In addition, ROS can promote the expression and release of cytokines and inflammatory mediators by damaging and activating RACs, muller cells, and microglia, which results in the destruction of the blood-retinal barrier and the homeostasis of the retinal environment and ultimately induces pathological vascular

proliferation (Moreli, Santos, Rocha, & Damasceno, 2014; Santiago et al., 2018). Thus, these observations indicate that the components of the neuroepithelial layer of the retina have a critical role in the mechanism of pathological retinal angiogenesis.

RACs are glial cells that are widely present in the retinal neuroepithelial layer, enveloping axons of ganglion cells and retinal microvessels and forming axons and vascular glial sheaths (Vecino et al., 2016). In some studies, RACs have been proved to participate in the formation of the blood-retinal barrier, transmission of signals, protection of nerve cells, maintenance of homeostasis and nutritional support (Hajrasouliha et al., 2013; Luna et al., 2016). Alterations in retinal homeostasis such as oxidative stress injury lead to astrocyte gliosis, a process characterized by a shift in the supportive role of astrocytes toward a pro-inflammatory state, which can regulate endothelial cell function and vascular permeability and finally lead to retinal vascular diseases (Dharmarajan et al., 2014; Schneider & Fuchshofer, 2016; Vecino et al., 2016). Therefore, our study explored in detail, for the first time, the effects of astrocytes of the retinal neuroepithelial layer on endothelial cell function under different states such as oxidative stress and their possible mechanism.

tBHP is an exogenous inducer of oxidative stress with several advantages over H_2O_2, such as high stability and slow release; it has been widely used to construct oxidative stress models for ROS-related diseases in vitro and could induce apoptosis and increase the ROS levels in the cells (Cai et al., 2016; Kaja et al., 2015). ROS-induced damage is mainly related to the mitochondrial damage-mediated apoptosis pathway (Antonetti et al., 2006; Qu et al., 2019; Zhong, Song, Pang, & Liu, 2018). Exogenous ROS or other injuries can destroy the DNA structure and organelle membranes, especially the mitochondrial membrane. Damage to the mitochondrial membrane leads to the release of endogenous ROS in the mitochondria, further aggravating the oxidative stress damage to the cells. This process can be reflected by the activation of the mitochondrial apoptotic pathway (Tao et al., 2016). In the present study, we used tBHP to induce oxidative stress injury in RACs. As shown in Figure 1, with increasing concentrations of tBHP, the survival rate of the cells obviously decreased, the morphology of the cells changed, membrane lipid peroxidation increased, intracellular ROS accumulation increased, and apoptosis pathway activation was enhanced in the cells.

4.2 | Oxidative stress can improve both autophagy and apoptosis responses in RACs and further enhance HUVEC functions in the transwell system

Autophagy has crucial roles during development and disease, and evidence indicates that autophagy also has a direct role in modulating aging and apoptosis (Hansen & Rubinsztein, 2018). Based on the previous studies (Pei et al., 2016; H. F. Wang et al., 2018), this correlation between ROS, autophagy, and apoptosis seems to be a dynamic relationship that is difficult to clarify. Generally, autophagy blocks the induction of apoptosis, and apoptosis-associated caspase activation shuts off the autophagic process (Marino, Niso-Santano,
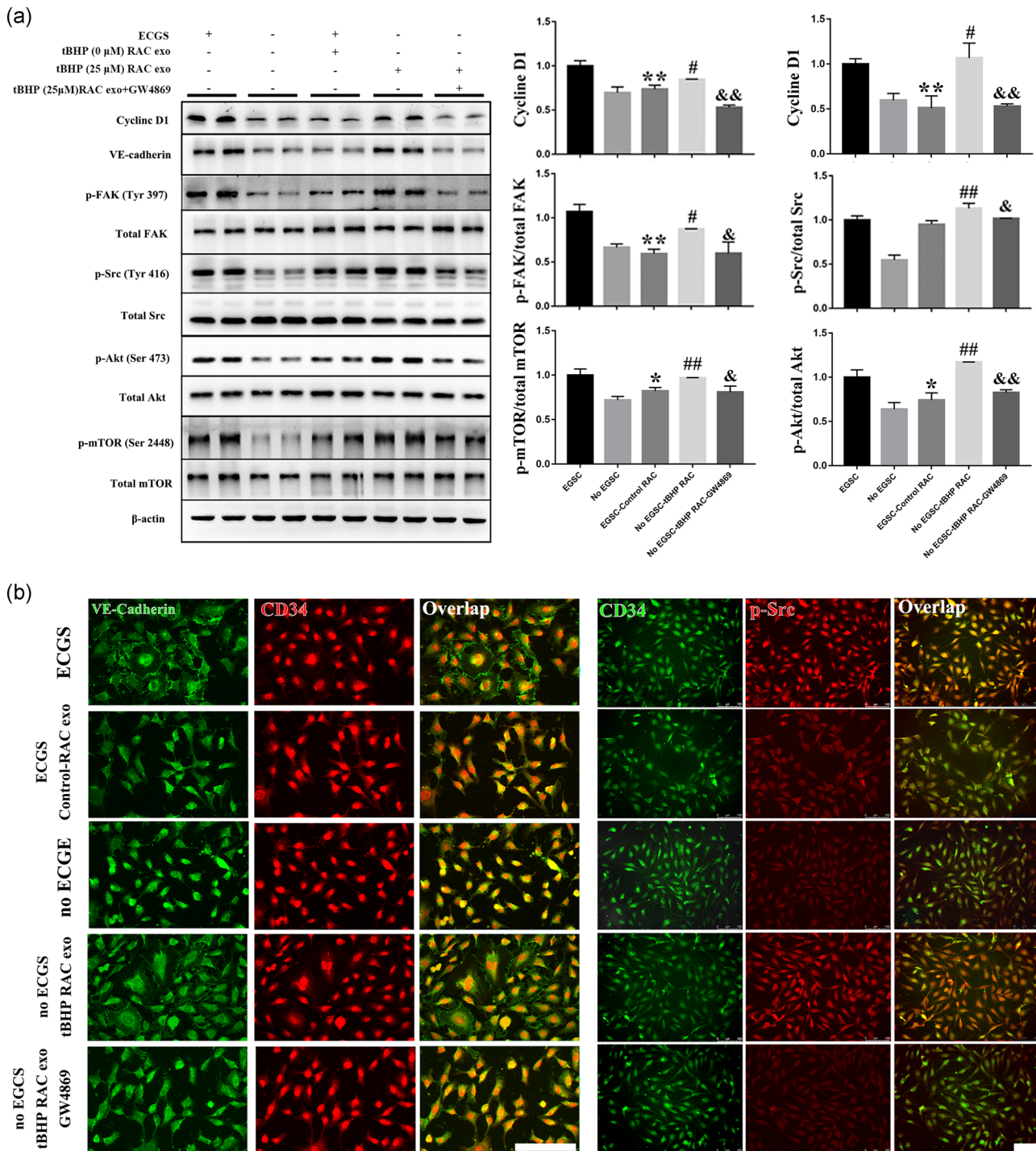
FIGURE 7 The proliferation- and migration-related pathways are highly inhibited by normal RAC exosomes and are enhanced by exosomes derived from RACs with high-autophagy levels. (a,b) The activity of the Src–FAK–Akt–mTOR pathway expression of cyclin D1 and VE-cadherin were reduced by normal RAC-derived exosomes when compared with the ECGS groups. However, the tBHP-RAC exosomes can obviously elevate the pathway activity expression of cyclin D1 and VE-cadherin compared with the no ECGS group. Moreover, GW4869 can block the tBHP-RAC exosome effects on the related pathway in HUVECs. Scale bar = 100 μm. The results are expressed as mean ± standard deviation. ECGS, endothelial cell growth supplement; FAK, focal adhesion kinase; HUVEC, human umbilical vein endothelial cell; mTOR, mammalian target of rapamycin; RAC, retinal astrocyte; tBHP, tert-butyl hydroperoxide; VE, vascular endothelial. *$p < .05$ and **$p < .01$ versus ECGS; #$p < .05$ and ##$p < .01$ versus no ECGS; &$p < .05$ and &&$p < .01$ versus no the ECGS-tBHP RAC group

Baehrecke, & Kroemer, 2014). Mitochondria are the main source of intracellular ROS, and Gilardini et al (Gilardini Montani et al., 2019) found that downregulating the transcription of mitochondrial DNA lead to a decrease in autophagy levels in EBV-infected monocytes, thereby switching the cells from differentiation to apoptosis. Moreover, reducing the autophagy level can activate the antioxidant response by the accumulation of SQSTM1/p62, ultimately causing a decrease in ROS to further inhibit autophagy and enhance apoptosis. However, in special cases, autophagy or autophagy-related proteins may help induce apoptosis or necrosis, and autophagy has been shown to degrade the cytoplasm excessively, leading to 'autophagic cell death' (Marino et al., 2014). In their research, Karna et al. (2010) found that a tubulin-binding noscapine analog could trigger the release of ROS, which further led to apoptosis in PC-3 cells. With the increase in apoptosis levels, a number of autophagic vacuoles could be observed in analog-treated PC-3 cells, as well as increased expression of LC3β and beclin-1, which were infrequently seen in controls. However, when ROS were eliminated, autophagy also decreased, which indicated that ROS are also involved in autophagy regulation. Therefore, there is a close relationship between ROS, autophagy and apoptosis, and they may work together and interact with each other.

In our research, we observed a synergistic effect. As the tBHP concentration increased, the number of TUNEL-positive cells remarkably increased, and the activation of Bcl-2 and caspase-3-dependent apoptosis was also increased. We also found that ROS levels also positively regulated autophagy. The expression of the autophagy-related pathway mTOR-p62-LC3 in RACs was significantly increased, and a significant accumulation of LC3β was also observed in tBHP-RACs. Moreover, the coexpression level of LC3β and LAMP1 was elevated, which indicated an increase in autolysosome number and an enhancement of cell autophagy responses (Jeppesen et al., 2019). Thus, the activity of both autophagy and apoptosis can be significantly enhanced by increasing ROS levels in our research (Figure 2).

Furthermore, in addition to participating in the stress response of cells, autophagy is also involved in the regulation of various physiological functions (Botbol, Guerrero-Ros, & Macian, 2016; Mortensen, Watson, & Simon, 2011; Orhon et al., 2016). It has been proven that autophagy activation can promote epithelial-to-mesenchymal transition (EMT) in colon cancer cells through beclin-1-related pathways, thereby promoting cell migration and invasion behaviors (Shen et al., 2018). W. Li, Li, Gao, and Yang (2018) found that the activation of autophagy promotes the migration and differentiation of HUMSCs by promoting the expression of the transcription factors SDF-1 and SOX-2, which played a crucial role in maintaining the pluripotency and proliferation of HUMSCs. In addition, autophagy has been found to regulate the proliferation and migration of human endothelial progenitor cells (hEPCs) by GABARAPL1 (Mo, Zhang, & Yang, 2016). Those studies suggest that increasing autophagy levels within certain limits can enhance cell function; however, other studies have observed different phenomena. Y. Wang et al. (2019) indicated that autophagy also functions to weaken the EMT program in RAS-mutated cancer cells by the SQSTM1-RELA pathway and inhibit RAS-induced cell migration and invasion. Therefore, the regulatory role of autophagy in cell processes is not constant even in similar situations. Certain factors may affect the regulation of autophagy. In their research, L. Li et al. (2019) found that a low glucose or glucose-free state promoted the migration and movement of keratinocytes, but both were suppressed under high glucose conditions, and they were shown to be regulated by the p38/MAPK autophagy pathway. It seems that the regulation of autophagy is highly context-dependent. Thus, the regulation of autophagy is not constant even for the same process under different conditions.

In our research, we observed the same phenomenon. When HUVECs were cocultured with RACs in a Transwell assay, we found that RACs exerted different effects under different conditions. The level of autophagy in RACs under normal conditions was at baseline, and these cells could reduce the migration and tube formation of HUVECs compared with the ECGS group (Figure 3). The results of western blot and immunofluorescence assays also showed that the activation of HUVEC migration-related pathways was decreased (Figure 4). However, when RACs suffered from oxidative stress injury, their ROS and autophagy levels were significantly upregulated. In addition, both wound closure and tube-forming experiments showed that RACs with high autophagy could significantly promote migration and tube formation processes and the related signaling pathways in HUVECs. However, when the autophagy inhibitor 3MA was added to RACs, the promoting effect was significantly reversed even in the case of oxidative damage (Figures 3 and 4). Therefore, we concluded that autophagy in RACs could regulate endothelial cell function. RACs with low autophagy levels inhibited HUVEC function, and when the autophagy in RACs was elevated, endothelial cell proliferation and migration were also enhanced. However, the specific mechanism to produce this kind of intercellular regulation is still unclear.

4.3 | The autophagy level of RACs is involved in the regulation of HUVEC function via exosomal-based delivery

Autophagy is a mechanism for the recycling and degradation of cytoplasmic content, and the autophagosome is the hallmark of this process. Cytosolic content can be sequestered into vesicles called autophagosomes, which then fuse either with lysosomes resulting in degradation, or with endosomes to form amphisomes, which then fuse with the plasma membrane leading to exocytosis of the content (Carta, Lavieri, & Rubartelli, 2013). Emanuele, Notaro, and Palumbo Piccionello (2018) found that the vacuolar H + ATPase inhibitor bafilomycin A1 (BafA1) could prevent the fusion between autophagosomes and lysosomes and further promote the secretion of cytosolic pro-IL-1β and regulate the function of the recipient cells. Therefore, autophagy may share similar molecular mechanisms with exocytosis and may be involved in the regulation of signal transmission between cells.

The exosome is a kind of microvesicle with a diameter of approximately 30–150 nm. Exosomes were once thought to be used to remove unwanted substances from the cells, but later research found that the exosomes released from cells contained large amounts of proteins, fats, nucleic acids, miRNAs, and circRNAs, and the exosomes could be taken up by targeted cells to released signal regulators, which could have powerful biological downstream effects (Mathieu & Martin-Jaular, 2019; Pluchino & Smith, 2019). After extensive research, exosomes have been found to be involved in many disease development mechanisms and play an important role. For example, MSC-derived exosomes have a protective effect on myocardial ischemia-reperfusion injury (Lai et al., 2010; Wei et al., 2019). The exosomes derived from neural stem cells can promote the repair and regeneration of neurovascular function (Zagrean, Hermann, Opris, Zagrean, & Popa-Wagner, 2018), and tumor cells mediate tumor metastasis through paracrine exosomes (Fujita, Yoshioka, & Ochiya, 2016).

Further study revealed that exosome generation and autophagosomes may be involved in similar mechanisms. Autophagy essential pathway autophagy-related genes (Atg) might serve as the critical factors, playing a central role in endocytosis, protein secretion, and vesicles transporting cytosolic content to lysosomes or vacuoles

(Manjithaya & Subramani, 2011; Shravage, Hill, Powers, Wu, & Baehrecke, 2013). Nonenveloped picornaviruses exit infected cells by hijacking Atg8/LC3-labeled autophagic membranes in a nonlytic manner by filamentous budding (Munz, 2017a). The inner autophagosome membrane and its content can also be secreted and might give rise to exosomes (Munz, 2017b). H. Guo et al. (2017) further proved that Atg is deeply involved in late endosome acidification to regulate the generation of exosomes, and lacking Atg5 and Atg16L1 can strongly reduce exosome production. The dynamic process of the evolution of autophagosomes and exosomes has been addressed in a recent study (Jeppesen et al., 2019), in which autophagosomes are shown to have two fates after generation. One is to envelop cargos and fuse with lysosomes to form the autolysosome, thus recycling substances after degradation. The other is to fuse with late endosomes or multivesicular endosomes to form the amphisome and further transport to the plasma membrane, releasing their contents into the extracellular space. It is known that the late endosome and multivesicular endosome are the precursors of microvesicles, including exosomes that carry specific molecular markers including CD63, while autophagosomes can be marked by LC3. Thus, exosomes can transport the cargo of autophagosomes by forming amphisomes, and we can observe the amphisomes by the colocalization of CD63
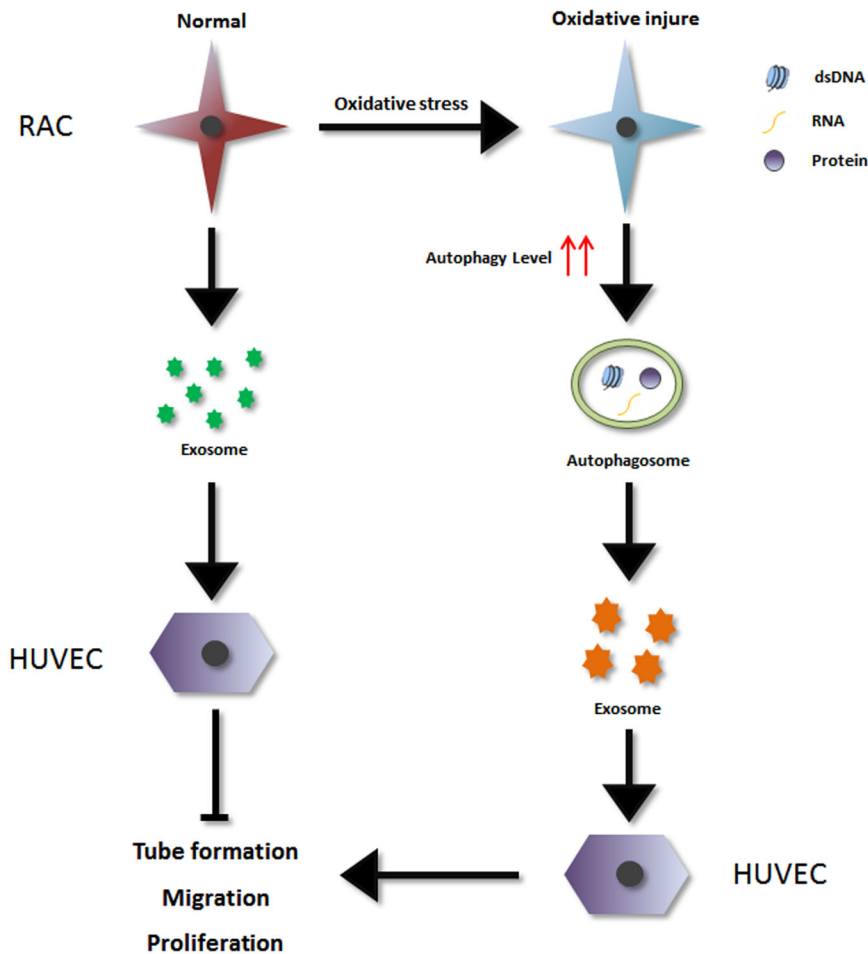

FIGURE 8 Oxidative stress-induced RAC autophagy can improve the HUVEC functions by releasing exosomes. Exosomes secreted by normal RAC can inhibit endothelial cell migration and tube formation; while the exosomes generated from oxidative stress-induced high-autophagy RAC can promote endothelial cell proliferation, migration, and tube formation. In addition, significant differences can be observed between the two sources exosomes. HUVEC, human umbilical vein endothelial cell; RAC, retinal astrocyte

and LC3 (Figure 5b) to access this process. Furthermore, exosomes extracted from different cell types or the same cells but under different physiological conditions have been shown to have different physical and chemical properties and transport different components (Hajrasouliha et al., 2013). This may be a potential mechanism for disease progression.

In our research, the exosomes, extracted by ultracentrifugation, derived from normal RACs and high-autophagy level RACs had entirely different effect on HUVEC migration and tube formation. The normal RAC-derived exosomes strongly inhibited HUVEC function, which is consistent with previous research (Hajrasouliha et al., 2013). However, under oxidative stress, as the level of autophagy in RACs increased, RAC-derived exosomes instead promoted the tube formation and migration of HUVECs (Figure 6). The results of western blot and immunofluorescence assays also indicated that cell proliferation and migration were enhanced (Figure 7). Interestingly, by identifying exosomes from control, tBHP and tBHP + 3MA, we found some potential clues to explain this phenomenon. The control exosomes had a smaller size and a higher abundance than high-autophagy RAC-derived exosomes. But, declining the autophagy level can further increase the amount of particle and enlarge their size. The reason of this phenomenon was not discussed in present study, further exploration can focus on this effect. However, the tBHP + 3MA exosome presented a similar characteristic with control exosome, which has a low HSP70 expression and high expressions of TSG101, CD81, and CD63 compared with high-autophagy RAC-derived exosomes. It indicated that tBHP-induced autophagy response was involved in the exosomal contents packaging and exosome synthesis. To further validate the role of exosomes in this regulation, we added the exosome inhibitor GW4869 to the oxidative RACs to block exosome release. The results showed that the RAC autophagy has almost no influence and the promoting effect induced by oxidative RAC exosomes on HUVECs was significantly attenuated (Figure 6). This result was also confirmed by immunofluorescence and western blot analysis (Figure 7). Therefore, we believe that the autophagy response is highly involved in the generation of RAC exosome under tBHP treatment, and tBHP treatment RAC-derived exosomes are a critical factor that regulates the proliferation and migration of HUVECs.

5 | CONCLUSION

In conclusion, this study indicated that oxidative injury induced RAC autophagy, which further upregulated migration- and proliferation-related pathways, ultimately affecting endothelial cell function. The RAC-derived exosomes are a critical factor in this process. Thus, RACs might transmit an autophagy-induced signal by releasing exosomes to regulate the proliferation and migration of endothelial cells, thereby participating in the mechanism of occurrence and development of retinal vascular-related diseases (Figure 8). As we observed in the present study, the exosomes generated from two sources had significant differences in features and function, and further study focusing on the differences in the cargo transported by the exosomes derived from the two sources is still necessary.

CONFLICT OF INTERESTS
The authors declare that they have no competing interests.

AUTHOR CONTRIBUTIONS
Z. J. X. designed the experiments; Z. L. X. performed the experiments; Z. J. K. revised the manuscripts and performed the supplementary experiments; L. B. and Y. G. C. contributed to the statistical analyses and interpretation; Z. L. X. drafted the manuscript, which was modified by H. L. L. and L. L. All authors read and approved the final manuscript.

DATA AVAILABILITY STATEMENT
All data generated or analyzed during this study are included in this article. And we have not used other data that has already been published. All the data presented in this article are original results derived from this study.

ORCID
Jingxiang Zhong http://orcid.org/0000-0002-5774-7602

REFERENCES
Antonetti, D. A., Barber, A. J., Bronson, S. K., Freeman, W. M., Gardner, T. W., Jefferson, L. S., … Simpson, I. A. (2006). Diabetic retinopathy: Seeing beyond glucose-induced microvascular disease. *Diabetes*, *55*(9), 2401–2411. https://doi.org/10.2337/db05-1635

Botbol, Y., Guerrero-Ros, I., & Macian, F. (2016). Key roles of autophagy in regulating T-cell function. *European Journal of Immunology*, *46*(6), 1326–1334. https://doi.org/10.1002/eji.201545955

Cai, L., Wang, L. F., Pan, J. P., Mi, X. N., Zhang, Z., Geng, H. J., … Luo, H. M. (2016). Neuroprotective Effects of methyl 3,4-dihydroxybenzoate against TBHP-induced oxidative damage in SH-SY5Y cells. *Molecules*, *21*(8), 1071. https://doi.org/10.3390/molecules21081071

Carta, S., Lavieri, R., & Rubartelli, A. (2013). Different members of the IL-1 family come out in different ways: DAMPs vs. cytokines? *Frontiers in Immunology*, *4*, 123. https://doi.org/10.3389/fimmu.2013.00123

Castillo, B., Jr., del Cerro, M., Breakefield, X. O., Frim, D. M., Barnstable, C. J., Dean, D. O., & Bohn, M. C. (1994). Retinal ganglion cell survival is promoted by genetically modified astrocytes designed to secrete brain-derived neurotrophic factor (BDNF). *Brain Research*, *647*(1), 30–36. https://doi.org/10.1016/0006-8993(94)91395-1

Corada, M., Liao, F., Lindgren, M., Lampugnani, M. G., Breviario, F., Frank, R., … Dejana, E. (2001). Monoclonal antibodies directed to different regions of vascular endothelial cadherin extracellular domain affect adhesion and clustering of the protein and modulate endothelial permeability. *Blood*, *97*(6), 1679–1684.

Dharmarajan, S., Gurel, Z., Wang, S., Sorenson, C. M., Sheibani, N., & Belecky-Adams, T. L. (2014). Bone morphogenetic protein 7 regulates reactive gliosis in retinal astrocytes and Muller glia. *Molecular Vision*, *20*, 1085–1108.

Dorrell, M. I., Aguilar, E., Jacobson, R., Trauger, S. A., Friedlander, J., Siuzdak, G., & Friedlander, M. (2010). Maintaining retinal astrocytes normalizes revascularization and prevents vascular pathology associated with oxygen-induced retinopathy. *GLIA*, *58*(1), 43–54. https://doi.org/10.1002/glia.20900

Emanuele, S., Notaro, A., & Palumbo Piccionello, A. (2018). Sicilian litchi fruit extracts induce autophagy versus apoptosis switch in human

colon cancer cells. *Nutrients*, 10(10), 1490. https://doi.org/10.3390/nu10101490

Fujita, Y., Yoshioka, Y., & Ochiya, T. (2016). Extracellular vesicle transfer of cancer pathogenic components. *Cancer Prevention Research*, 107(4), 385–390. https://doi.org/10.1111/cas.12896

Gilardini Montani, M. S., Santarelli, R., Granato, M., Gonnella, R., Torrisi, M. R., Faggioni, A., & Cirone, M. (2019). EBV reduces autophagy, intracellular ROS and mitochondria to impair monocyte survival and differentiation. *Autophagy*, 15(4), 652–667. https://doi.org/10.1080/15548627.2018.1536530

Guo, B., Huang, J., Wu, W., Feng, D., Wang, X., Chen, Y., & Zhang, H. (2014). The nascent polypeptide-associated complex is essential for autophagic flux. *Autophagy*, 10(10), 1738–1748. https://doi.org/10.4161/auto.29638

Guo, H., Chitiprolu, M., Roncevic, L., Javalet, C., Hemming, F. J., Trung, M. T., ... Gibbings, D. (2017). Atg5 disassociates the V1V0-ATPase to promote exosome production and tumor metastasis independent of canonical macroautophagy. *Developmental Cell*, 43(6), 716–730. https://doi.org/10.1016/j.devcel.2017.11.018

Hajrasouliha, A. R., Jiang, G., Lu, Q., Lu, H., Kaplan, H. J., Zhang, H. G., & Shao, H. (2013). Exosomes from retinal astrocytes contain antiangiogenic components that inhibit laser-induced choroidal neovascularization. *Journal of Biological Chemistry*, 288(39), 28058–28067. https://doi.org/10.1074/jbc.M113.470765

Hansen, M., & Rubinsztein, D. C. (2018). Autophagy as a promoter of longevity: Insights from model organisms. *Nature Reviews: Molecular Cell Biology*, 19(9), 579–593. https://doi.org/10.1038/s41580-018-0033-y

Henkind, P. (1964). Hyperbaric oxygen and corneal neovascularisation. *Lancet*, 2(7364), 836–838. https://doi.org/10.1016/s0140-6736(64)90687-7

Igarashi, Y., Chiba, H., Utsumi, H., Miyajima, H., Ishizaki, T., Gotoh, T., ... Sawada, N. (2000). Expression of receptors for glial cell line-derived neurotrophic factor (GDNF) and neurturin in the inner blood-retinal barrier of rats. *Cell Structure and Function*, 25(4), 237–241.

Jammalamadaka, A., Suwannatat, P., Fisher, S. K., Manjunath, B. S., Hollerer, T., & Luna, G. (2015). Characterizing spatial distributions of astrocytes in the mammalian retina. *Bioinformatics*, 31(12), 2024–2031. https://doi.org/10.1093/bioinformatics/btv097

Jeppesen, D. K., Fenix, A. M., Franklin, J. L., Higginbotham, J. N., Zhang, Q., Zimmerman, L. J., ... Coffey, R. J. (2019). Reassessment of exosome composition. *Cell*, 177(2), 428–445. https://doi.org/10.1016/j.cell.2019.02.029

Kaja, S., Payne, A. J., Naumchuk, Y., Levy, D., Zaidi, D. H., Altman, A. M., ... Koulen, P. (2015). Plate reader-based cell viability assays for glioprotection using primary rat optic nerve head astrocytes. *Experimental Eye Research*, 138, 159–166. https://doi.org/10.1016/j.exer.2015.05.023

Karna, P., Zughaier, S., Pannu, V., Simmons, R., Narayan, S., & Aneja, R. (2010). Induction of reactive oxygen species-mediated autophagy by a novel microtubule-modulating agent. *Journal of Biological Chemistry*, 285(24), 18737–18748. https://doi.org/10.1074/jbc.M109.091694

Lai, R. C., Arslan, F., Lee, M. M., Sze, N. S., Choo, A., Chen, T. S., ... Lim, S. K. (2010). Exosome secreted by MSC reduces myocardial ischemia/reperfusion injury. *Stem Cell Research*, 4(3), 214–222. https://doi.org/10.1016/j.scr.2009.12.003

Li, L., Zhang, J., Zhang, Q., Zhang, D., Xiang, F., Jia, J., ... Huang, Y. (2019). High glucose suppresses keratinocyte migration through the inhibition of p38 MAPK/autophagy pathway. *Frontiers in Physiology*, 10, 24. https://doi.org/10.3389/fphys.2019.00024

Li, W., Li, K., Gao, J., & Yang, Z. (2018). Autophagy is required for human umbilical cord mesenchymal stem cells to improve spatial working memory in APP/PS1 transgenic mouse model. *Stem Cell Research & Therapy*, 9(1), 9. https://doi.org/10.1186/s13287-017-0756-2

Lin, W. J., & Kuang, H. Y. (2014). Oxidative stress induces autophagy in response to multiple noxious stimuli in retinal ganglion cells. *Autophagy*, 10(10), 1692–1701. https://doi.org/10.4161/auto.36076

Lindenbergh, M. F. S., & Stoorvogel, W. (2018). Antigen presentation by extracellular vesicles from professional antigen-presenting cells. *Annual Review of Immunology*, 36, 435–459. https://doi.org/10.1146/annurev-immunol-041015-055700

Luna, G., Keeley, P. W., Reese, B. E., Linberg, K. A., Lewis, G. P., & Fisher, S. K. (2016). Astrocyte structural reactivity and plasticity in models of retinal detachment. *Experimental Eye Research*, 150, 4–21. https://doi.org/10.1016/j.exer.2016.03.027

Manjithaya, R., & Subramani, S. (2011). Autophagy: A broad role in unconventional protein secretion? *Trends in Cell Biology*, 21(2), 67–73. https://doi.org/10.1016/j.tcb.2010.09.009

Marino, G., Niso-Santano, M., Baehrecke, E. H., & Kroemer, G. (2014). Self-consumption: The interplay of autophagy and apoptosis. *Nature Reviews Molecular Cell Biology*, 15(2), 81–94. https://doi.org/10.1038/nrm3735

Matei, I., Kim, H. S., & Lyden, D. (2017). Unshielding exosomal RNA unleashes tumor growth and metastasis. *Cell*, 170(2), 223–225. https://doi.org/10.1016/j.cell.2017.06.047

Mathieu, M., & Martin-Jaular, L. (2019). Specificities of secretion and uptake of exosomes and other extracellular vesicles for cell-to-cell communication. *Nature Cell Biology*, 21(1), 9–17. https://doi.org/10.1038/s41556-018-0250-9

Meng, W., Hao, Y., He, C., Li, L., & Zhu, G. (2019). Exosome-orchestrated hypoxic tumor microenvironment. *Molecular Cancer*, 18(1), 57. https://doi.org/10.1186/s12943-019-0982-6

Mo, J., Zhang, D., & Yang, R. (2016). MicroRNA-195 regulates proliferation, migration, angiogenesis and autophagy of endothelial progenitor cells by targeting GABARAPL1. *Bioscience Reports*, 36(5), https://doi.org/10.1042/bsr20160139

Moreli, J. B., Santos, J. H., Rocha, C. R., & Damasceno, D. C. (2014). DNA damage and its cellular response in mother and fetus exposed to hyperglycemic environment. *BioMed Research International*, 2014, 676758. https://doi.org/10.1155/2014/676758

Mortensen, M., Watson, A. S., & Simon, A. K. (2011). Lack of autophagy in the hematopoietic system leads to loss of hematopoietic stem cell function and dysregulated myeloid proliferation. *Autophagy*, 7(9), 1069–1070. https://doi.org/10.4161/auto.7.9.15886

Munz, C. (2017a). The autophagic machinery in viral exocytosis. *Frontiers in Microbiology*, 8, 269. https://doi.org/10.3389/fmicb.2017.00269

Munz, C. (2017b). Autophagy proteins in viral exocytosis and anti-viral immune responses. *Viruses*, 9(10), 288. https://doi.org/10.3390/v9100288

Murillo, O. D., Thistlethwaite, W., Rozowsky, J., Subramanian, S. L., Lucero, R., Shah, N., ... Milosavljevic, A. (2019). exRNA atlas analysis reveals distinct extracellular RNA cargo types and their carriers present across human biofluids. *Cell*, 177(2), 463–477.e415. https://doi.org/10.1016/j.cell.2019.02.018

Orhon, I., Dupont, N., Zaidan, M., Boitez, V., Burtin, M., Schmitt, A., ... Codogno, P. (2016). Primary-cilium-dependent autophagy controls epithelial cell volume in response to fluid flow. *Nature Cell Biology*, 18(6), 657–667. https://doi.org/10.1038/ncb3360

Pei, J., Deng, J., Ye, Z., Wang, J., Gou, H., Liu, W., ... Chen, J. (2016). Absence of autophagy promotes apoptosis by modulating the ROS-dependent RLR signaling pathway in classical swine fever virus-infected cells. *Autophagy*, 12(10), 1738–1758. https://doi.org/10.1080/15548627.2016.1196318

Periyasamy, P., & Shinohara, T. (2017). Age-related cataracts: Role of unfolded protein response, Ca(2+) mobilization, epigenetic DNA modifications, and loss of Nrf2/Keap1 dependent cytoprotection. *Progress in Retina and Eye Research*, 60, 1–19. https://doi.org/10.1016/j.preteyeres.2017.08.003

Pluchino, S., & Smith, J. A. (2019). Explicating exosomes: Reclassifying the rising stars of intercellular communication. *Cell*, *177*(2), 225–227. https://doi.org/10.1016/j.cell.2019.03.020

Prattichizzo, F., Micolucci, L., Cricca, M., De Carolis, S., Mensa, E., Ceriello, A., ... Olivieri, F. (2017). Exosome-based immunomodulation during aging: A nano-perspective on inflamm-aging. *Mechanisms of Ageing and Development*, *168*, 44–53. https://doi.org/10.1016/j.mad.2017.02.008

Provis, J. M. (2001). Development of the primate retinal vasculature. *Progress in Retina and Eye Research*, *20*(6), 799–821.

Qu, D., Jiang, M., Huang, D., Zhang, H., Feng, L., Chen, Y., ... Han, J. (2019). Synergistic effects of the enhancements to mitochondrial ROS, p53 activation and apoptosis generated by aspartame and potassium sorbate in HepG2 cells. *Molecules*, *24*(3), 457. https://doi.org/10.3390/molecules24030457

Santiago, A. R., Boia, R., Aires, I. D., Ambrosio, A. F., & Fernandes, R. (2018). Sweet stress: Coping with vascular dysfunction in diabetic retinopathy. *Frontiers in Physiology*, *9*, 820. https://doi.org/10.3389/fphys.2018.00820

Sapieha, P., Hamel, D., Shao, Z., Rivera, J. C., Zaniolo, K., Joyal, J. S., & Chemtob, S. (2010). Proliferative retinopathies: Angiogenesis that blinds. *International Journal of Biochemistry and Cell Biology*, *42*(1), 5–12. https://doi.org/10.1016/j.biocel.2009.10.006

Schneider, M., & Fuchshofer, R. (2016). The role of astrocytes in optic nerve head fibrosis in glaucoma. *Experimental Eye Research*, *142*, 49–55. https://doi.org/10.1016/j.exer.2015.08.014

Seen, S., & Tong, L. (2018). Dry eye disease and oxidative stress. *Acta Ophthalmologica*, *96*(4), e412–e420. https://doi.org/10.1111/aos.13526

Shen, H., Yin, L., Deng, G., Guo, C., Han, Y., Li, Y., ... Zeng, S. (2018). Knockdown of beclin-1 impairs epithelial-mesenchymal transition of colon cancer cells. *Journal of Cellular Biochemistry*, *119*(8), 7022–7031. https://doi.org/10.1002/jcb.26912

Shravage, B. V., Hill, J. H., Powers, C. M., Wu, L., & Baehrecke, E. H. (2013). Atg6 is required for multiple vesicle trafficking pathways and hematopoiesis in Drosophila. *Development*, *140*(6), 1321–1329. https://doi.org/10.1242/dev.089490

Tang, M. K. S., Yue, P. Y. K., & Ip, P. P. (2018). Soluble E-cadherin promotes tumor angiogenesis and localizes to exosome surface. *Nature Communications*, *9*(1), 2270. https://doi.org/10.1038/s41467-018-04695-7

Tao, Y., Geng, L., Xu, W. W., Qin, L. M., Peng, G. H., & Huang, Y. F. (2016). The potential utilizations of hydrogen as a promising therapeutic strategy against ocular diseases. *Therapeutics and Clinical Risk Management*, *12*, 799–806. https://doi.org/10.2147/tcrm.s102518

Thery, C., Ostrowski, M., & Segura, E. (2009). Membrane vesicles as conveyors of immune responses. *Nature Reviews Immunology*, *9*(8), 581–593. https://doi.org/10.1038/nri2567

Ung, L., Pattamatta, U., Carnt, N., Wilkinson-Berka, J. L., Liew, G., & White, A. J. R. (2017). Oxidative stress and reactive oxygen species: A review of their role in ocular disease. *Clinical Science*, *131*(24), 2865–2883. https://doi.org/10.1042/cs20171246

van Wijngaarden, P., Coster, D. J., & Williams, K. A. (2005). Inhibitors of ocular neovascularization: Promises and potential problems. *Journal of the American Medical Association*, *293*(12), 1509–1513. https://doi.org/10.1001/jama.293.12.1509

Vecino, E., Rodriguez, F. D., Ruzafa, N., Pereiro, X., & Sharma, S. C. (2016). Glia-neuron interactions in the mammalian retina. *Progress in Retina and Eye Research*, *51*, 1–40. https://doi.org/10.1016/j.preteyeres.2015.06.003

Wang, H. F., Wang, Z. Q., Ding, Y., Piao, M. H., Feng, C. S., Chi, G. F., ... Ge, P. F. (2018). Endoplasmic reticulum stress regulates oxygen-glucose deprivation-induced parthanatos in human SH-SY5Y cells via improvement of intracellular ROS. *CNS Neuroscience & Therapeutics*, *24*(1), 29–38. https://doi.org/10.1111/cns.12771

Wang, Y., Xiong, H., Liu, D., Hill, C., Ertay, A., Li, J., ... Miller, P. (2019). Autophagy inhibition specifically promotes epithelial-mesenchymal transition and invasion in RAS-mutated cancer cells. *Autophagy*, *15*(5), 886–899. https://doi.org/10.1080/15548627.2019.1569912

Wei, Z., Qiao, S., Zhao, J., Liu, Y., Li, Q., Wei, Z., ... Xu, B. (2019). miRNA-181a over-expression in mesenchymal stem cell-derived exosomes influenced inflammatory response after myocardial ischemia-reperfusion injury. *Life Sciences*, *232*, 116632. https://doi.org/10.1016/j.lfs.2019.116632

Wisniewska-Kruk, J., Hoeben, K. A., Vogels, I. M., Gaillard, P. J., Van Noorden, C. J., Schlingemann, R. O., & Klaassen, I. (2012). A novel co-culture model of the blood-retinal barrier based on primary retinal endothelial cells, pericytes and astrocytes. *Experimental Eye Research*, *96*(1), 181–190. https://doi.org/10.1016/j.exer.2011.12.003

Xu, X. L., Lee, T. C., Offor, N., Cheng, C., Liu, A., Fang, Y., ... Cobrinik, D. (2010). Tumor-associated retinal astrocytes promote retinoblastoma cell proliferation through production of IGFBP-5. *American Journal of Pathology*, *177*(1), 424–435. https://doi.org/10.2353/ajpath.2010.090512

Zagrean, A. M., Hermann, D. M., Opris, I., Zagrean, L., & Popa-Wagner, A. (2018). Multicellular crosstalk between exosomes and the neurovascular unit after cerebral ischemia. Therapeutic implications. *Frontiers in Neuroscience*, *12*, 811. https://doi.org/10.3389/fnins.2018.00811

Zhang, N., Kolesnikov, A. V., Jastrzebska, B., Mustafi, D., Sawada, O., Maeda, T., ... Palczewski, K. (2013). Autosomal recessive retinitis pigmentosa E150K opsin mice exhibit photoreceptor disorganization. *Journal of Clinical Investigation*, *123*(1), 121–137. https://doi.org/10.1172/jci66176

Zhong, H., Song, R., Pang, Q., & Liu, Y. (2018). Propofol inhibits parthanatos via ROS-ER-calcium-mitochondria signal pathway in vivo and vitro. *Cell Death & Disease*, *9*(10), 932. https://doi.org/10.1038/s41419-018-0996-9